Journal of Inorganic and General Chemistry
ZAAC
Zeitschrift für anorganische und allgemeine Chemie
DOI: 10.1002/zaac.202000286
ARTICLE

Spin States of 1D Iron(II) Coordination Polymers with Redox Active $TTF(py)_2$ as Bridging Ligand

Sophie Schönfeld,[a] Gerald Hörner,[a] Frank W. Heinemann,[b] Anja Hofmann,[c] Roland Marschall,[c] and Birgit Weber*[a]

Dedicated to Prof. Thomas Klapötke on the Occasion of his 60th Birthday

Abstract. In this manuscript, we report the solvent-dependent synthesis of 1D coordination polymers derived from two planar N_2O_2-coordinate iron(II) complexes **FeL1** and **FeL2**, which incorporate $TTF(py)_2$ as a bridging bis-monodentate ligand. The obtained 1D polymers were characterized through elemental analysis, Mössbauer spectroscopy, single crystal structure analysis for **2a**·2 DMF, magnetic susceptibility measurements, X-ray powder diffraction, cyclic voltammetry and diffuse reflectance spectroscopy, supplemented by DFT computation. The results revealed additive electronic properties of the sub-units FeL and $TTF(py)_2$ with only minor mutual influence. Intriguingly however, the solvent-of-synthesis is found to be a steering factor of the magnetic spin crossover properties of the resulting materials, yielding divergent behavior if obtained from DMF, MeCN or EtOH. This becomes strikingly evident for the magnetic properties of the DMF-derived polymer which is found trapped in the low-spin state in the single crystal **2a**· 2 DMF, but shows a gradual spin crossover if all solvent is removed.

1 Introduction

In recent years, the research of molecular magnetic materials has increased in interest due to the application potential in spintronics, memory devices or molecular actuators.[1,2] Switchable coordination compounds are extensively studied as building blocks of such functional molecular materials, often relying on spin crossover (SCO) between energetically close lying spin states. It is, by now, well established that octahedral complexes with an iron(II) metal center can be switched between the paramagnetic high spin ($S = 2$) and diamagnetic low spin ($S = 0$) state by external stimuli such as temperature, pressure or light, provided suitable ligands were selected.[3–5] To address the multifaceted challenges of today's life, it is desirable to design materials that offer multifunctionality by integrating several properties. The combination of spin crossover with several additional effects realizes molecular sensors and actuators which can be controlled in a targeted manner.[2,5,6] First important steps towards multifunctional materials have been made through the investigation of additional properties such as magnetic exchange interactions,[7] photoluminescence[8] or lipid layer like packing through long alkyl chains leading to phase transitions.[9] More recent studies have focused on the integration of SCO in redox-active materials.[10,11] Especially for a possible application in data storage devices, electrical conductivity is an interesting feature of the material.[12]

A promising candidate to realize a linkage between conductivity, redox activity and spin crossover is tetrathiafulvalene (TTF) that is known for its excellent electron-donating properties.[10,13–15] The diverse chemistry of TTF began 1973 by discovering the first organic metal TTF-TCNQ (TCNQ = tetracyanoquino-dimethane),[16] making use of the reversible oxidation of TTF to the stable radical cation ($TTF^{\bullet+}$) and the dication (TTF^{2+}).[17] While mononuclear complexes incorporating TTF moieties have been known for a while, it was only very recently that incorporation into iron(II)-based coordination polymers with ligand-appended TTF was reported.[13,14] In both studies the Schiff base-like equatorial ligand system established by *Weber* and *Jäger* et al. is used, known for its variety of spin transitions.[3,18,19,20] As a large number of interesting iron(II) coordination polymers with descendants of bidentate pyridine-containing ligands is known,[3,18,21] the ligand 2,6(7)-bis(4-pyridyl)-1,4,5,8-tetrathiafulvalene ($TTF(py)_2$) reported 2007 by *Han* et al., is an interesting aspirant for the synthesis of coordination polymers combining SCO behavior and redox active properties.[22,23] The combination of these two systems in a 1D coordination polymer, has recently been

* Prof. Dr. B. Weber
E-Mail: weber@uni-bayreuth.de
[a] Inorganic Chemistry IV
University of Bayreuth
Universitätsstraße 30
95448 Bayreuth, Germany
[b] Department Chemie und Pharmazie
Friedrich-Alexander-Universität Erlangen-Nürnberg
Egerlandstraße 1
91058 Erlangen, Germany
[c] Physical Chemistry III
University of Bayreuth
Universitätsstraße 30
95448 Bayreuth, Germany
Supporting information for this article is available on the WWW under **http://dx.doi.org/10.1002/zaac.202000286** or from the author.

communicated to be successful[24] and will be further deepened in the course of this work. Herein we investigate the impact of solvents used during the synthesis of two different coordination polymers on their magnetic properties.

2 Results and Discussion

2.1 Synthesis of Coordination Polymers $\{[FeL1/2(TTF(py)_2)]\}_n$

The redox active ligand $TTF(py)_2$ was synthesized as described in the literature.[22,25,26] Coordination polymers were formed in a one-pot reaction from equimolar mixtures of the mononuclear iron(II) complexes $[FeL1/2(MeOH)_2]$ and the bridging ligand $TTF(py)_2$. The iron(II) precursors were obtained as oxygen-sensitive fine crystalline powders as described previously.[27] L1/L2 denotes the remote substitution pattern with R = $-CH_3$ and $-OCH_3$ for L1 and L2, respectively (Scheme 1). The polymer synthesis was carried out in three different solvents, *N*,*N*-dimethylformamide (DMF), ethanol (EtOH), and acetonitrile (MeCN) at elevated temperature (Table 1). Whereas the iron(II) precursor is well soluble in all three solvents, the bridging ligand is reasonably soluble only in DMF and EtOH, but shows a rather low solubility in MeCN. In the latter medium, the solid product **1b/2b** is therefore obtained in a reprecipitation reaction from solid $TTF(py)_2$; complete turnover in this case is assigned visually with respect to the markedly different color of reactant and product. In Scheme 1, the general synthesis of the complexes is displayed. The desired products could be obtained from all three solvents used giving satisfying elemental analysis in solvent-free formulations for **1b**, **1c** and **2a**–**2c**. Reproduction of the compounds in the respective medium always provided the same elemental analysis results. The synthesis, single-crystal X-ray structure and solid-state redox properties of **1c** have been recently communicated,[24] but will be covered in more detail with regard to the properties in solution herein.

It was only for **1a** obtained from DMF, where we observed a significant deviation from a solvent-free 1:1 stoichiometry of FeL1/2 and $TTF(py)_2$, pointing to the presence of additional DMF molecules in the fine crystalline product. Thermogravimetric analysis (see Figure S1, Supporting Information) indeed revealed significant thermal weight losses of ca. 6.5 % between 80 °C $< \vartheta <$ 120 °C for **1a**; that corresponds to 0.7 molecules DMF per formula unit. Intriguingly, this behavior is not observed in powder samples of **2a**, which differs from **1a** only in substitution of a side group. Nevertheless, single crystalline material obtained from **2a** likewise proves the presence of uncoordinated DMF molecules in the solid state (see below). As DMF clearly is the most potent donor among the solvents used,[28] coordination towards the metal center, if in part, cannot be ruled out for the powder sample.[28,29]

2.2 Single Crystal X-ray Structure Analysis

Crystals suitable for X-ray structure analysis of **2a** were obtained directly from the DMF synthesis solution; it is hereinafter referred to as **C2a**. The crystallographic data were obtained at 100 K and 273 K and are summarized in Table S1 (Supporting Information). The coordination polymer **C2a** crystallizes in the triclinic space group $P\bar{1}$ with two formula units in the unit cell. The ORTEP drawing together with the used

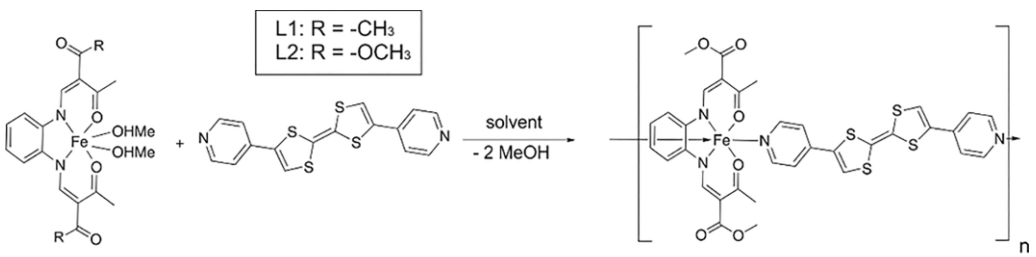

Scheme 1. General synthesis of the iron(II) coordination polymer $\{[FeL_x(TTF(py)_2)]\}_n$ and used abbreviations.

Table 1. Overview of the solvents used during synthesis and corresponding results of the elemental analysis. The calculated values correspond to the solvent-free formulation.

	Results elemental analysis (1) $C_{34}H_{28}FeN_4O_4S_4$	Solvent		Results elemental analysis (2) $C_{34}H_{28}FeN_4O_6S_4$
1a [a]	C: 53.86 H: 4.29 N: 8.69 S: 17.11	DMF	**2a**	C: 52.16 H: 3.88 N: 7.88 S: 16.19
1b	C: 55.18 H: 3.76 N: 7.48 S: 16.96	MeCN	**2b**	C: 52.22 H: 3.71 N: 7.06 S:16.55
1c	C: 54.70 H: 3.98 N: 7.69 S: 17.41	EtOH	**2c**	C: 52.57 H: 3.95 N: 7.17 S: 16.03
	C: 55.13 H: 3.81 N: 7.56 S: 17.32	expected		C: 52.85 H: 3.65 N: 7.25 S: 16.60

a) Formulation indicated by elemental analysis: $C_{34}H_{28}FeN_4O_4S_4 \cdot 0.7\ C_3H_7NO$.

atom numbering scheme is displayed in Figure 1. Within each monomeric repeat unit, two molecules of DMF are detected. The oxygen atom O3 of the free ester group is disordered at 100 K. The co-crystallized DMF molecules are also disordered at both temperatures. The C=C bond length of the TTF unit of the axial ligand is a good indicator for the oxidation state of the ligand. With a bond length of 1.34 Å at 100 K and 273 K, the $TTF(py)_2$ ligand is at both temperatures in the non-oxidized, neutral state.[30]

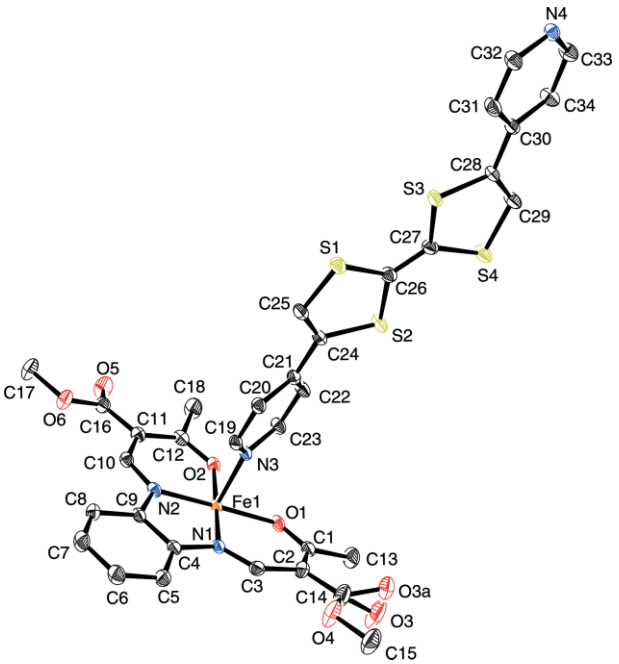

Figure 1. ORTEP drawing of the asymmetric unit of **C2a** (100 K) with the atom numbering scheme used in the text, co-crystallized solvent molecules are omitted for clarity. Thermal ellipsoids presented at 50 % level. Hydrogen atoms are omitted for clarity (for ORTEP drawing of the asymmetric unit of **C2a** (100 K) with co-crystallized solvent see Figure S2, Supporting Information).

The octahedral N_4O_2 coordination sphere of the iron(II) center consists of the Schiff base-like equatorial ligand and the axially bridging ligand $TTF(py)_2$ that is bound through the terminal pyridyl groups. Selected bond lengths and angles within the inner coordination sphere are summarized in Table 2. **C2a** is clearly in the LS state at 100 K, considering the average Fe–N bond lengths of 1.90 Å and an O_{eq}–Fe–O_{eq} angle of 87.8°.[3,18] Heating to 273 K only leads to minor changes in bond lengths and angles around the central metal; thus the spin state is conserved. (see Figure S3, Supporting Information). Strikingly, the previously published crystals of **1c** conserve the HS state down to 100 K.[24]

The crystal packing of **C2a** at 100 K is displayed in Figure 2a and b; as temperature variation has only minor effects the discussion is focused on the low-temperature data. In the rich literature on solid-state structures of TTF derivatives, stacking of adjacent TTF units is a recurrent motif which often dominates among the non-covalent interactions and serves to define the packing.[14,31,32] For instance, the single crystals of the recently reported iron(II) coordination polymer **1c**,[24] feature extensive stacking of adjacent TTF units. By contrast, TTF units do not stack among themselves in **C2a**. Several short intermolecular contacts are observed as summarized in Table S2 (Supporting Information). A closer look at the packing pattern of **C2a** reveals that the polymer strands are arranged in opposite directions (Figure 2c). Following the Miller direction (*h k l*), one polymer strand is oriented in direction (0 1 –1) and the other in direction (0 –1 1). The Schiff base-like equatorial unit is organized in a slightly staggered fashion while the phenylene backbones of two polymer strands point in opposite directions. The co-crystallized solvent DMF seems to play a decisive role for the packing. A total of five hydrogen bonds can be identified in which one of the DMF molecules is involved. Predominantly contacts to the axial $TTF(py)_2$ ligands occur. This involves both the TFF unit (C36–H36B···S4 / C25–H25···O7) and the coordinating pyridyl rings (C31–H31··· O8 / C34–H34···O8A[b]).

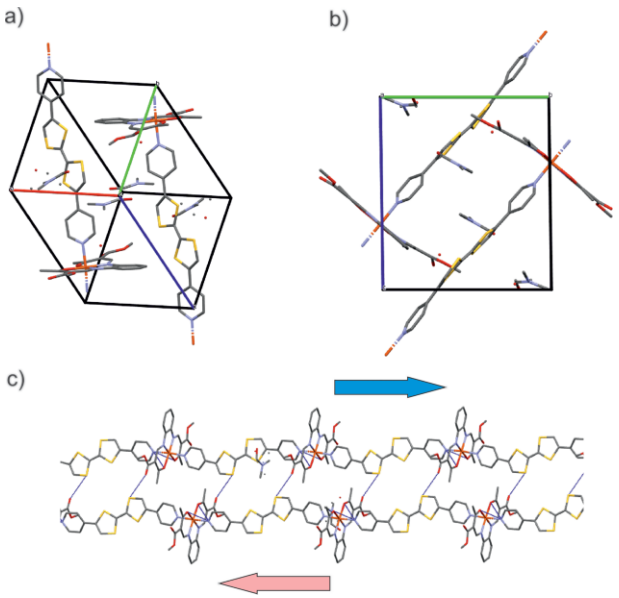

Figure 2. Molecular packing of compound **C2a** in the crystal at 100 K. (a) View along unit cell direction [1 1 1] and (b) view along unit cell direction [1 0 0] (c) Excerpt of two polymer strands with the interchain contacts given as dashed line. Hydrogen atoms are omitted for clarity.

Table 2. Selected bond lengths /Å and angles /° within the inner coordination sphere of the iron(II) complex **C2a** at 100 K and 273 K.

T /K	Fe–N_{eq}	Fe–O_{eq}	Fe–N_{ax}	O_{eq}–Fe–O_{eq}	N_{ax}–Fe–N_{ax}
100	1.900 (2)	1.936 (18)	1.984 (2)	87.79 (8)	175.34 (9)
	1.905 (2)	1.937 (18)	1.991 (2)		
273	1.903 (3)	1.940 (2)	1.994 (3)	88.29 (10)	175.35 (11)
	1.905 (3)	1.943 (2)	2.004 (3)		

2.3 Mössbauer Spectroscopy

^{57}Fe Mössbauer spectra were collected from the polymers **1a**–**1c** and **2a**–**2c** to validate the purity of the samples and to specify the spin state of the powdered samples at room temperature. As a representative example the spectrum of **2c** is displayed in Figure 3, the spectra of the other complexes are given in Figure S4 (Supporting Information). All spectra show one doublet with a quadrupole splitting $\Delta E_Q \approx 2.2$ mm·s^{-1} and an isomer shift $\delta \approx 0.9$ mm·s^{-1}. These values are in the range typical of high-spin iron(II) complexes of this ligand type.[3] The presence of μ-oxido impurities as a notorious thermodynamic sink in the presence of dioxygen can be safely ruled out through the absence of signals at $\Delta E_Q = 0.80$ and $\delta \approx 0.30$ mm·s^{-1} and the rather symmetric doublets. The Mössbauer parameters are summarized in Table 3. The exclusive HS configuration is at odds with the results from the single-crystal structure of **C2a**, which is clearly low-spin at 273 K. Slightly changed synthesis conditions under which **C2a** was obtained compared to **2a** (see Experimental Section) and differences in the elemental composition could be an explanation for the different magnetic properties. Unfortunately, it was not possible to record a Mössbauer spectrum of **C2a** or to perform a magnetic susceptibility measurement, because only a few small crystals were obtained.

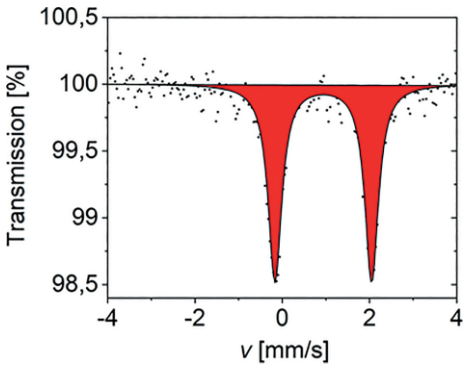

Figure 3. Exemplary Mössbauer spectrum of **2c**. The relative transmission is plotted against the speed of the source.

Table 3. Parameters of the hyperfine interactions of **{[FeL1/2(TTF(py)$_2$)]}$_n$** obtained from either DMF (a), MeCN (b), or EtOH (c). The spectra were recorded at room temperature.

	Spin state	δ /mm·s^{-1}	ΔE_Q /mm·s^{-1}	Γ/2 /mm·s^{-1}
1a	HS	0.936(12)	2.19(2)	0.221(19)
1b	HS	0.903(17)	2.15(3)	0.27(3)
1c	HS	0.95(3)	2.22(6)	0.19(4)
2a	HS	0.94(4)	2.23(8)	0.18(3)
2b	HS	0.935(12)	2.20(2)	0.217(18)
2c	HS	0.940(10)	2.21(2)	0.189(16)

2.4 Magnetic Susceptibility Measurements and X-ray Powder Diffraction

Magnetic susceptibility measurements in the temperature range from 400 K to 50 K allow a more detailed investigation of the magnetic properties of the compounds **1a**–**1c** and **2a**–**2c** to address the different spin states obtained from SC-XRD and Mössbauer spectroscopy. Heating-cooling sequences in the order 300 K → 50 K → 400 K → 50 K → 300 K were used for all samples. The results of these measurements reveal similar, but slightly different behavior, as illustrated in Figure 4. In fact, SCO occurs in all powdered materials but remains incomplete.

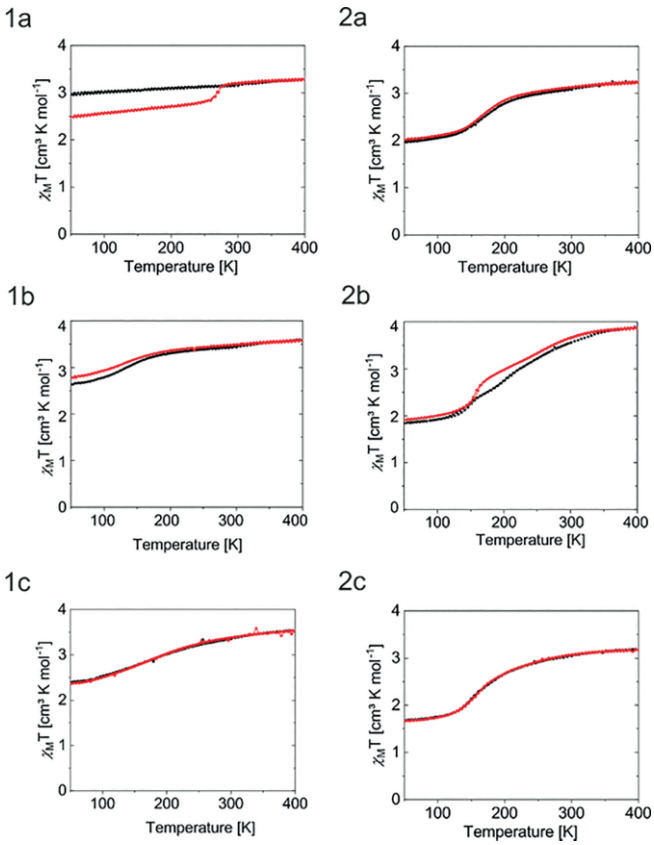

Figure 4. Plot of the $\chi_M T$ product vs. temperature in the range 400–50 K with a cooling rate of 5 K·min^{-1}. Black curve: cooling and heating between 300 K and 50 K, and red curve: cooling and heating between 400 K and 50 K.

Upon cooling, in all cases a decrease in the $\chi_M T$ values is detectable. Characteristic individual values are listed in Table 4. At room temperature, all compounds exhibit $X_M T$ products around 3.15 ± 0.15 cm^3·K·mol^{-1}. The magnetic moment is in a range typical for a high spin iron (II) coordination compound with an octahedral environment.[3]

Table 4. $\chi_M T$ product for **{[FeL1/2(TTF(py)$_2$)]}$_n$** obtained from either DMF (a), MeCN (b) or EtOH (c). Values are given for different temperatures (300, 50, 400 K) and at 50 K after one heating cycle to 400 K.

	$\chi_M T$ product 300 K	$\chi_M T$ product 50 K	$\chi_M T$ product 400 K	$\chi_M T$ product 50 K after heating
1a	3.15	2.96	3.27	2.48
1b	3.43	2.63	3.57	2.78
1c	3.35	2.39	3.52	2.39
2a	3.07	1.96	3.24	2.01
2b	3.55	1.84	3.85	1.91
2c	3.04	1.67	3.17	1.66

The small differences in the SCO behavior between **2b** [γ_{HS}(50 K) = 0.50 (red) 0.48 (black)] and the relatively similar **2c** [γ_{HS}(50 K) = 0.53] on the one hand and **2a** [γ_{HS}(50 K) = 0.61] on the other is reflected by small differences in crystal packing as becomes evident from the powder XRD patterns given in Figure 5. Firstly, co-crystallization of free TTF(py)$_2$ can be safely ruled out, based on the absence of prominent reflections of the axial ligand (e.g. at 8.6°). Secondly the reflexes recorded of **2b** and **2c** are highly similar, pointing to a conserved packing of the polymers if derived from MeCN and EtOH. By contrast the pattern of **2a** differs significantly due to the presence of DMF in the lattice. It is furthermore noted that the PXRD pattern of powdered **2a** likewise differs significantly from the implications of the crystal structure of **C2a** (black and red curves in Figure 5). The PXRD patterns of **1a**–**1c** are given in Figure S5 (Supporting Information). In line with the results of the magnetic measurements, the differences in these measurements are reflected by differences in the PXRD patterns. It is important to note that the axial ligand used can be in the *cis* as well as in the *trans* configuration. Accordingly, there is the possibility that both isomers are involved in polymer formation in different proportions. The preference for one of the two isomers under the given reaction conditions, such as the boiling point of the solvent used, could also lead to small differences in magnetic behavior.

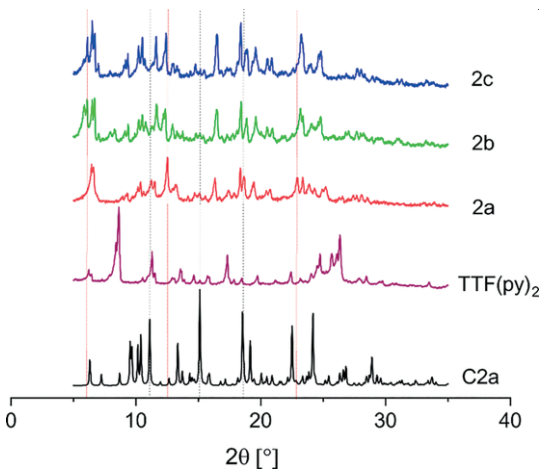

Figure 5. PXRD pattern of the coordination polymers, **2a**–**2c** and the axial ligand TTF(py)$_2$ in the angular range of 2θ = 5–30° at room temperature; for comparison a computed PXRD pattern derived from single-crystalline **C2a** at 100 K is shown.

2.5 UV/Vis Diffuse Reflectance Spectra

The optical properties of the samples were addressed with UV/Vis diffuse reflectance spectroscopy in order to resolve possible differences among the different batches. The red-brown color of the powder samples along series **2** translates into reflectivity spectra analogous to the one shown for **2a** in Figure 6, blue line. In a broad spectral range from 1200–600 nm the reflectivity continuously decreases, indicating significant light absorption across a wide range of the visible spectrum. Further analysis of the spectrum was conducted using Kubelka-Munk theory [Equation (1)][33] to process the reflectivity data into the $F(R)$ parameter which is proportional to the optical absorption coefficient [Equation (1); $R = k/s$; k and s: absorption and scattering coefficient; red in Figure 6]. Significant bands at 675, 539 and 493 nm which dominate the visible color impression can be identified in all materials (for **2b/c** see Figure S6, Supporting Information).

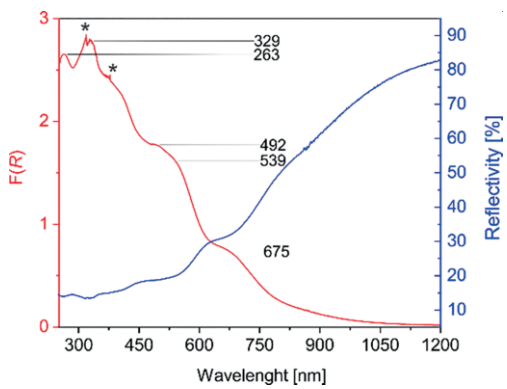

Figure 6. Reflectivity of **2a** which was optically diluted 1:4 with $BaSO_4$ (blue line). Kubelka-Munk converted diffuse reflectance spectrum according to Equation (1) (red line). Asterisks denote small discontinuities due to lamp and filter change of the spectrometer.

The absorption in this area is mainly attributed to the TTF chromophores contained in the complex matrix. Since this is identical for all materials regardless of the solvent used, it can be assumed that essentially the same coordination polymer is formed in all three cases.

$$F(R) = \frac{(1-R)^2}{2R} \quad (1)$$

However, the small differences between the individual materials become clear again when the diffuse reflection spectrum of the near-infrared range of the undiluted samples is considered (Figure S7, Supporting Information). The band structure here is basically similar in all three samples examined. However, an additional band at 1861 nm can be identified in **2a**, which cannot be found in **2b/c**. Thus, once again the presence of DMF in the powder of **2a** is a differentiating factor.

Finally, we note that the failure of **1** and **2** to undergo complete SCO in the powder is not due to a molecule-borne limitation. As is shown exemplarily for **2c**, the systems are generally able to perform a complete spin crossover in solution. Upon cooling to liquid nitrogen temperature, all filtrates from the polymer syntheses show characteristic color changes from red brown to intense purple as shown in Figure 7. The room temperature color and the impression at low temperature are con-

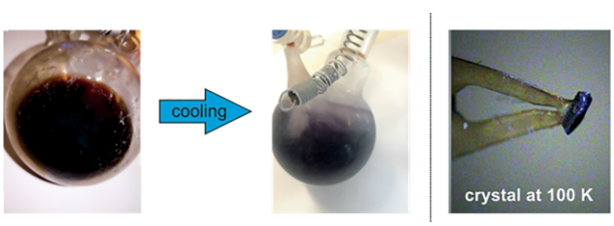

Figure 7. Color change of the filtrate of **2c** upon cooling with liquid nitrogen. As a comparison, the single crystal **C2a** at 100 K is shown.

Table 5. Metrics of the inner coordination sphere in the crystal structure of $\{$**[FeL1(TTF(py$_2$)]**$\}_n$ and DFT-optimized metrics in the dinuclear model complex **[(py)L1Fe(TTF(py$_2$)FeL1(py)]** in three global spin states S = 0, 2 and 4.[a) c)].

	Exp. **C2a** (100K/ 273K)	Exp. **C1c** [b)] (100 K)	Singlet		Quintet		Nonet	
			Fe(a)	Fe(b)	Fe(a)	Fe(b)	Fe(a)	Fe(b)
Fe–N_{eq}	1.90/ 1.91	2.127	1.90	1.90	1.91	2.11	2.11(1)	2.10(5)
Fe–O_{eq}	1.94/ 1.94	2.051	1.95	1.95	1.95	2.04	2.04	2.03
Fe–N_{ax}	1.99/ 2.00	2.279	2.00	2.00(1)	2.00	2.25(5)	2.26(5)	2.27(4)
Fe···Fe	18.7/ 18.7	–	18.5		18.9		19.1	
>C=C<	1.34/ 1.34	1.345(3)	1.35		1.35		1.35	
cis O_{eq}–Fe–O_{eq}	87.8/ 88.3	112.7/115.1	90.4	89.3	90.0	114.8	116.0	112.3
trans N_{ax}–Fe–N_{ax}	175.3/ 175.3	–	176.9	176.5	174.5	170.0	170.3	177.0
trans N_{eq}–Fe–O_{eq}	178.5/ 178.4 177.9/ 178.0	–	177.3(2)	178.0(1)	177.5	161.2(1)	160.9(4)	162.8(1)

a) Optimized with BP86-D3/TZVP/COSMO. b) From solid-state structure of $\{$[FeL2(TTF(py$_2$)]$\}_n$ in Reference.[24] c) A rotation by 90° of neighbored [FeN_2O_2] units corresponds to the situation in **C1c**; it is noted that the energy difference between rotated and eclipsed constellations is not significant.

sistent with SCO as they closely match results reported and analyzed recently for a related system.[13] At 100 K the single crystal **C2a** has the same color as the cooled filtrate as can be seen in Figure 7. Unfortunately, it was not possible for us to trace the color changes using UV/Vis spectroscopy by cooling a solution as the axial ligand dissociates at the required concentrations. For this reason, we decided to use DFT-based structural modeling to better understand the behavior of the complex.

2.6 DFT Structure Modelling

To analyse the steric requirements of SCO along a polymer strand in more detail, we performed a DFT-inquiry in the molecular structures and spin-state dependent energies of truncated binuclear model compounds. To this end, we introduce a dinuclear iron(II) complex **[(py)L1Fe(TTF(py$_2$)FeL1(py)]**, which conserves the experimental setting with respect to equatorial ligand L1 and bridging ligand TTF(py)$_2$ [L1 was used herein instead of L2 to avoid complications due to notorious rotation of the flexible –C(O)OMe group]. At the terminal axial positions of Fe(a) and Fe(b) we placed pyridine molecules as a close mimic of the ligand properties of TTF(py)$_2$. This approach complements a recent theoretical study wherein we approximated the electronic properties of polymer **1** as the mononuclear complex [FeL1(pyTTF)$_2$], carrying two axially coordinated TTF units.[24] The metrics were optimized with the BP86 functional and large TZVP basis sets. This setting has been found suitable to match the metrics of iron(II) complexes in a number of previous cases.[13] The optimized structure of **[(py)L1Fe(TTF(py$_2$)FeL1(py)]** in the all-low spin electron configuration corresponding to singlet multiplicity with S = 0 closely matches the experimental metrics of **C2a** (Table 5).

Similarly, the all-high spin structure of **[(py)L1Fe(TTF(py$_2$)FeL1(py)]** fully matches the implications of **C1c** (Figure 8; structure plot of S = 2 is given on Figure S8, Supporting Information). Importantly, the intrachain distance Fe···Fe of 18.7 Å in the crystal is very well matched by the dinuclear model if treated in the all-low spin state S = 0. Selected metrical data obtained for all spin states are compared with experimental data in Table 5. It is noted that an increase of overall spin in the models from S = 0 to S = 2 indicates localized structural response; that is, Fe(a) and Fe(b) become dissymmetric with local configurations of S = 0 and S = 2, respectively. The finding of electronic asymmetry is significant and reliable and rules out the possible formation of intermediate-spin centers with S = 1 both on Fe(a) and Fe(b); the inherently asymmetric electronic structure of **[(py)L1Fe(TTF(py$_2$)FeL1(py)]** therefore overrides the well-known tendency of the BP86 functional towards symmetric formulations.[34]

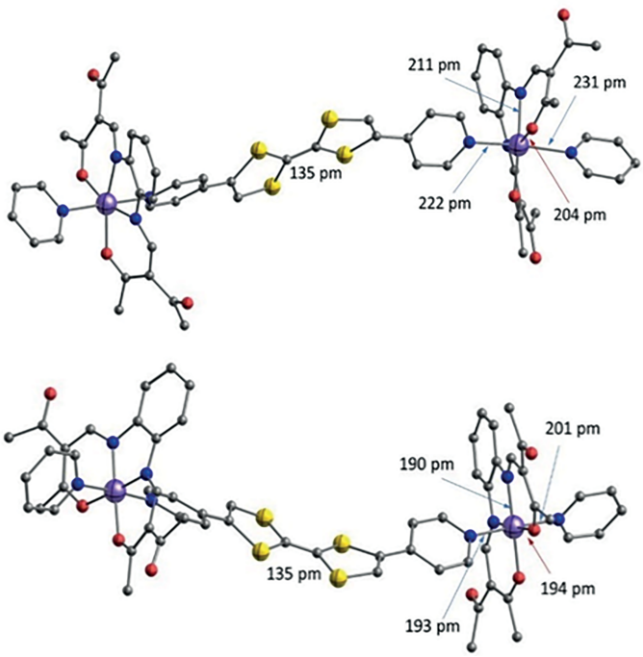

Figure 8. DFT-optimized structure of the dinuclear model [(py)L1Fe(TTF(py)$_2$)FeL1(py)] in the all-high spin state, S = 8/2 (top) and in the all-low spin state, S = 0 (bottom).

Structural changes due to SCO largely reflect isotropic breathing of the iron-donor bonds by up to $\Delta d \approx 0.2$ Å as is typically observed for iron(II) complexes in general[3,6,10] and

specifically for the Schiff base-like N_4O_2 environment.[3,18,20] Breathing along the intra-chain z-axis leads to expansion/contraction of the Fe···Fe distance in the dinuclear model by ≈ 0.6 Å, similar values prevail when **C1c** (HS) and **C2a** (LS) are compared. That means that complete SCO of all iron(II) centers along a given chain in the crystal must lead to massive strain build-up.

2.7 Electronic Structure: Theory and Experiment

The conserved SCO energy computed in this work for **[FeL1(py)$_2$]** and **[(py)L1Fe(TTFpy$_2$)FeL1(py)]** suggests the presence of decoupled electrophores, TTF and iron(II). In fact, recent work had shown that a TTF unit remains electronically unaffected by an iron(II) center if incorporated in the equatorial ligand L;[14] conserved electrochemical potentials had reflected an additive frontier orbital pattern of undisturbed metal-borne and TTF-borne contributions. Intriguingly, closer inspection of the dinuclear model compound **[(py)L1Fe(TTFpy$_2$)FeL1(py)]** reveals that axially appended TTF units significantly affect the orbital energies. Figure 9 highlights the highest occupied MOs of the py-terminated mononuclear complex (left), of the bridging TTF ligand (right) and of the dinuclear complex with an embedded TTF bridge.

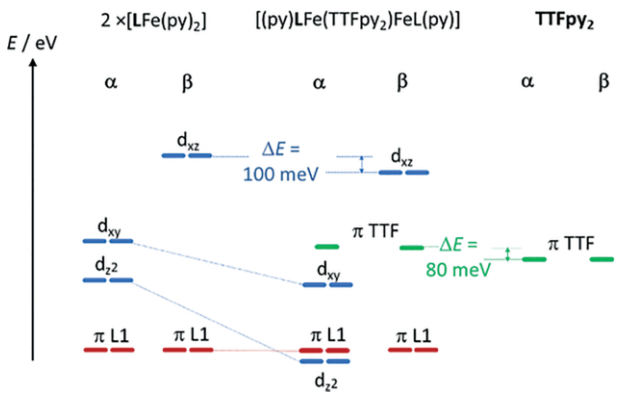

Figure 9. Character and energetic order of the highest occupied MOs; blue: metal-centred; red: centred on the equatorial ligand L1; green: TTF centred.

Referring to the experimental findings for powdered samples the complexes are in $S = 2$ (mononuclear) and $S = 4$ states (dinuclear), respectively (a corresponding diagram for the $S = 0$ case is given in Figure S9, Supporting Information). Color in the plot denotes the predominant character of the MO. Firstly, the metal-*d*-character of the highest occupied MO remains unaffected by the presence of either axial pyridine or TTFpy$_2$. (Electro-)chemical oxidation therefore must be expected to be metal borne.

Interestingly however, the coordination of TTFpy$_2$ acts as to significantly stabilize all orbitals with significant *d*-character by up to 400 meV; in particular stabilization of the largely non-bonding redox-active β-HOMO (d_{xz}) amounts to ca. 100 meV. In zero order (neglecting charge redistribution and/or SCO after oxidation), this shift suggests oxidation of the dinuclear complex (and of the coordination polymer **1**) to be significantly disfavored with respect to mononuclear **[L1Fe(py)$_2$]**. Indeed cyclovoltammetric studies, given in Figure 10, reveal an anodic shift of the iron(II/III) couple by ca. 100 mV if axially decorated with TTF(py)$_2$ across the entire series **1** and **2**; the iron(II/III) couple in **[L2Fe(py)$_2$]** resides at $E_{1/2} = -0.395$ V,[13] whereas the values of 1 and 2 crowd at $E_{1/2} \approx -0.28$ V.

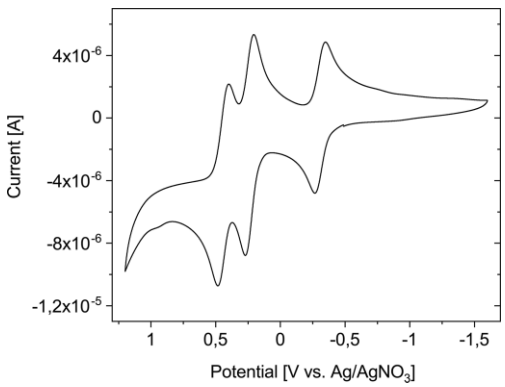

Figure 10. Cyclic voltammogram of **1a** in DMF with tetrabutylammonium hexafluorophosphate (NBu_4PF_6) (0.1 M) as supporting electrolyte on a platinum working and counter electrode at 50 mV·s^{-1} with a non-aqueous Ag/AgNO$_3$ reference electrode.

Electrochemical characteristics of all complexes were investigated by cyclic voltammetry (CV) at room temperature with dimethyl formamide (DMF) as solvent. For all measurements a non-aqueous Ag/AgNO$_3$ (c_{Ag^+} = 10 mM) reference electrode was used. Figure 10 exemplarily shows the curve recorded for **2a**. The cyclic voltammograms of all the other compounds investigated, look similar and are given in Figure S10 (Supporting Information). Since the concentration of the examined solution in cyclovoltammetric measurements is many times higher than in UV/Vis measurements, a dissociation of the axial ligand is unlikely, and an intact polymer can be expected. Each complex exhibits three one-electron redox couples. Half wave potentials and peak-to-peak separations are listed in Table 6.

The first half-wave potential of the six different complexes $E_{1/2}{}^1$ can be assigned to the redox process Fe^{2+}/Fe^{3+}. For all compounds these values are in agreement with investigations of similar systems by *Jäger* et al.[35] Both more anodic redox couples correspond to the oxidation of the TTF(py)$_2$ ligand to the radical-cation (TTF(py)$_2{}^{\bullet+}$) $E_{1/2}{}^2$ and in a second step to the dication (TTF(py)$_2{}^{2+}$) $E_{1/2}{}^3$ (Table 6). The potentials of the first oxidation of coordinate TTF(py)$_2$ match the free ligand for all iron(II) coordination compounds.[25] The peak-to-peak separations (Table 6) are in a range typical for either a reversible or a quasi-reversible redox process.[35,36] All half-wave potentials are stable over numerous measuring cycles (see Figure S11, Supporting Information); for this reason follow-up chemistry of the oxidized species can be ruled out. It cannot be completely excluded that even at higher concentrations of the coordination polymer, a ligand exchange with the solvent used does occur. It can be assumed that this only has a negligible effect, if at all, on the measurements carried out, since the half-wave potentials differ characteristically from the starting

Table 6. Half-wave potentials and peak-to-peak separations for complex **1a**–**1c**, **2a**–**2c** and $TTF(py)_2$. The peak-to-peak separation in the table refers to a scan rate of 50 mV·s^{-1}.

	$E_{1/2}{}^1$ /mV	$E_{1/2}{}^2$ /mV	$E_{1/2}{}^3$ /mV	ΔE_1 /mV	ΔE_2 /mV	ΔE_3 /mV
1a	–308	238	441	81	66	84
1b	–282	267	469	99	63	90
1c	–284	265	463	84	59	79
2a	–302	238	437	66	55	67
2b	–265	267	468	96	59	73
2c	–294	266	464	96	60	82
$TTF(py)_2$	–	138	339	–	63	75
$[FeL2(MeOH)_2]$	–388	–	–	68	–	–

materials used and the products obtained. However, for further studies it would be interesting to perform electrochemical and conductive measurements of the compounds in the solid state.

2.9 Discussion

There are already several examples demonstrating that the choice of solvent is not trivial for the synthesis of coordination polymers of the general type $[Fe(LN_2O_{2eq})(L_{ax})]_n$, as co-crystallized solvent molecules can have a significant impact on the magnetic properties.[20] In keeping with this, it became evident in elemental analysis and was also proven by thermogravimetric investigations that solvent inclusion is relevant for the coordination polymers discussed here. These differences go beyond the effect of remote ligand substitution but rather reflect major effects of the solvent selection on the crystal packing. The finding of a conserved low-spin state of **C2a** at both 100 K and 273 K was a surprise for two reasons: First, magnetic properties of powdered samples of **2a**–**2c** indicated pure high-spin character at room temperature and only partial crossover to the low-spin state at $T = 50$ K. Second, a previously reported single-crystal **C1c**·$(EtOH)_x$ obtained from EtOH is entirely high-spin at 100 K and 250 K.[24] It is well known that in order to perform spin crossover, a system must have enough flexibility to be able to make the necessary changes to the bond lengths.[3] The DMF molecules crystallized in the case of **C2a** are involved in crucial intra- and intermolecular contacts. These interactions may be one of the reasons for the sideways offset arrangement of the polymer strands and, accordingly, the TTF units. As a result, no stacking of TTF units, as described before in literature,[23,32,37] can be observed. The strong interaction with the DMF molecules may also well be responsible for the different magnetic behavior of the single crystal material **C2a** and the solvent-free powdered product **2a**.

For all samples it can be noted that upon cooling the magnetic moment decreases to an extent which clearly depends both on the substitution pattern (series **1** vs. **2**) and the solvent of synthesis (**a**, **b**, **c**). In general, samples derived from ligand series L2 host more complete SCO, although it must be noted that in none of the materials the low-spin fraction at $T = 50$ K goes below $\gamma_{LS} > 0.50$. As computation of the singlet-quintet splitting of the model complexes $[FeL1(py)_2]$ and $[FeL2(py)_2]$ with the TPSSh functional indicates, an only very mild influence of ligand substitution on the ligand-field strength is expected (difference in SCO energy: $\Delta\Delta_{SCO}E = 0.1$ kJ·mol^{-1}). We ascribe this differential effect on SCO of lateral –C(O)Me and –C(O)OMe substitution between series **1** and **2** largely to different packing effects.

Using DFT, we examined the changes in the intra-chain Fe···Fe distance during spin transition. The studies indicated that a spin transition is accompanied by a massive build-up of tension within the polymer strains. We think that packing-frustrated contraction/expansion may contribute to the observed hindrance of SCO in the bulk. Nevertheless, alternative explanations may be given for the incomplete SCO in bulk **{[FeL1(TTF(py)$_2$)]}$_n$** which is seen in SQUID magnetometry. The bridging $TTF(py)_2$ ligand is not in plane but shows a slight curvature. A spin-state dependent change of an axial bond length within the coordination center therefore requires an additional reorientation of the bonds within the axial ligand. Thus, in the polymer chain, the bond contraction due to SCO might be hindered. In a follow-up work we will investigate, if through the synthesis of nanoparticles those strain effects can be reduced.[38]

After having identified fine differences in the materials from different solvents by diffuse reflection spectroscopy and powder diffraction, differences in the electrochemical behavior also became apparent. While the overall pattern is similar for all polymers, the ones obtained from DMF, **1a** and **2a**, consistently show lower half-wave potentials for all three redox events. This might be read to be caused by variable average chain lengths of the polymers under the action of the varying donor numbers of the used solvents.[28,29] In this sense, it is clearly more likely in DMF than in the weaker donors EtOH and MeCN that the terminal iron(II) centers are coordinated by DMF rather than a $TTFpy_2$ molecule; this would indeed rationalize shorter chains in **1a** and **2a**, a notion which is corroborated by the deviating PXRD pattern of **2a**.

3 Conclusions

In this work the synthesis of new 1D coordination polymers is described that integrate the spin-state variability of iron(II) in the field of a Schiff base-like N_2O_2 ligand and the redox activity of a bis-monodentate bridging ligand. The ligand $TTF(py)_2$ with its interesting electrochemical behavior was used with the aim to synthesize iron(II) SCO complexes combined with redox active properties. Due to the poor solubility of the axial ligand $TTF(py)_2$ the synthesis was carried out in a selection of solvents with different reaction conditions. Elec-

trochemical studies by cyclic voltammetry reveal three (quasi-) reversible one-electron events involving the iron center and the tetrathiafulvalene unit and demonstrate the successful combination of an electronically switchable bridge with an iron(II) center. Intriguingly, small but significant differences in the magnetic and electrochemical behavior of the derived polymers could be observed despite the conserved bulk chemical composition.

Crystal structure analysis, *X*-ray powder diffraction and diffuse reflection spectroscopy aided in a preliminary rationalization and pointed to a high susceptibility of the polymer properties towards the presence and the relative number of solvent molecules in the lattice. In single crystalline material **C2a**, the presence of two DMF molecules in the unit cell acts to trap the LS state up to $T = 273$ K. By contrast, as-synthesized powders of **2a** with a residual lattice solvation of 0.7 DMF molecules per unit are likewise trapped, but in the high spin state. If the synthesis is performed in MeCN or EtOH, no co-crystallized solvent can be identified, resulting in high spin formulations. Divergent X-ray powder diffraction pattern suggest that it is indeed the divergent packing in the solid, which translates into solvent-of-synthesis dependent properties.

4 Experimental Section

If not stated otherwise all reactions were carried out using Schlenk technique with fresh degassed or distilled solvents. The axial ligand $TTF(py)_2$ was prepared according to literature procedures.[21] Chemicals used for synthesis were commercially available and used as received. Elemental analysis has been conducted with a Unicube from Elementar with sulfanilamide as standard. The samples were placed in a small tin boat. Mass spectra were recorded with a Finnigan MAT 8500 with a data system MASPEC II. Magnetic measurements were done on a MPMS-XL SQUID magnetometer from Quantum Design. The samples were put in a gelatine capsule and placed in a straw.

^{57}Fe Mössbauer Spectroscopy: The spectra were recorded in transmission geometry at constant acceleration using a conventional Mössbauer spectrometer with a 50 mCi ^{57}Co(Rh) source. The samples were prepared under argon atmosphere. Isomer shift values were reported with respect to α-Fe as a reference at room temperature.

Diffuse Reflection Measurements: Data were recorded on a PerkinElmer Lambda 750 UV/Vis/NIR spectrometer. A Praying-Mantis unit from Harrick was used for the measurements. The undiluted samples were calibrated with a Spektralon tablet and the diluted samples with $BaSO_4$ from Alfa Aesar. At 379.2 nm a filter change from filter BG38 to filter UG11 takes place and at 319.2 nm a lamp and filter change occur from filter UG11 at $T = 100$ %. At 860.8 nm there is a detector switch for the NIR region.

X-ray Crystal Structure Analysis: A suitable single crystal was embedded in protective perfluouropolyalkylether oil and transferred to the cold nitrogen gas stream of the diffractometer. Intensity data of **C2a** were collected at 100 K and 273 K using Mo-K_α irradiation (λ = 0.71073 Å) on a Bruker Kappa PHOTON 2 $I\mu S$ Duo diffractometer equipped with QUAZAR focusing Montel optics. Data were corrected for Lorentz and polarization effects; semi-empirical absorption corrections were performed on the basis of multiple scans using SADABS.[15] The structures were solved by direct methods (SHELX XT 2014/5)[39a] and refined by full-matrix least-squares procedures on F^2 using SHELXL 2018/3.[39b] Material for publication was prepared using OLEX2.[40] All non-hydrogen atoms were refined with anisotropic displacement parameters. In the crystal structure of **C2a** at 100 K the oxygen (O3) of one keto group was disordered. Two alternative orientations were refined and resulted in site occupancies of 54(2) and 46(2) % for O3 and O3A, respectively. The compound crystallized with two molecules of DMF (dimethyl formamide), one of which was disordered. Two alternative orientations were refined and resulted in site occupancies of 49.7(6) and 50.3(6) % for the atoms O8, N6, C38 – C40 and O8A, N6A, C38A – C40A, respectively. Similarity restraints were applied to the anisotropic displacement parameters of the disordered atoms. In the crystal structure of **C2a** at 273 K the disorder of oxygen O3 was no longer observed. Instead, both of the co-crystallized DMF solvent molecules were disordered. Two alternative orientations each were refined and resulted in site occupancies of 40.5(8) and 59.5(8) % for the atoms O7, N5, C35 – C37 and O7A, N5A, C35A – C37A, and of 46.3(13) and 53.7(13) % for the atoms O8, N6, C38 – C40 and O8A, N6A, C38A – C40A respectively. Similarity restraints were applied to the anisotropic displacement parameters of the disordered atoms. Additional pseudo-isotropic restraints were applied to the anisotropic displacement parameters of the disordered atoms of DMF O8 – C40 and O8A – C4A, respectively. All hydrogen atoms were placed in positions of optimized geometry; their isotropic displacement parameters were tied to those of the corresponding carrier atoms by a factor of either 1.2 or 1.5.

Crystallographic data (excluding structure factors) for the structures in this paper have been deposited with the Cambridge Crystallographic Data Centre, CCDC, 12 Union Road, Cambridge CB21EZ, UK. Copies of the data can be obtained free of charge on quoting the depository numbers CCDC-2017572 (for **C2a** at 100 K) and CCDC-2017571 (for **C2a** at 273 K) (Fax: +44-1223-336-033; E-Mail: deposit@ccdc.cam.ac.uk, http://www.ccdc.cam.ac.uk).

Cyclic Voltammetry: Cyclic voltammetry measurements were performed with an Electrochemical Analyzer CHI610E from CH Instruments in a three-electrode setup with a platinum working and counter electrode and a $Ag/AgNO_3$ non-aqueous reference electrode filled with the solvent used and tetrabutylammonium hexafluorophosphate as conducting salt.

{[FeL1(TTF(py)$_2$)]}$_n$

Synthesis in DMF (1a): A solution of $[FeL1(MeOH)_2]$ (0.2 g, 0.45 mmol) and $TTF(py)_2$ (0.17 g, 0.48 mmol) in DMF (15 mL) was heated to reflux for 2 h. After cooling and leaving to stand at 8 °C for 48 h, a dark red solid precipitated. The dark reddish powder was filtered off, washed with methanol two times (2 mL) and dried in vacuo to give $\{[FeL1(TTF(py)_2)]\cdot(0.7\ DMF)\}_n$ (yield 0.13 g, 41.3 %) $C_{35}H_{30}FeN_4O_4S_4\cdot 0.7C_3H_7NO$ (791.88 g·mol^{-1}): calcd. C 54.76, H 4.19, N 8.31, S 16.19 %; found: C 53.86, H 4.29, N 8.69, S 17.11 %. **MS** (DEI-(+), 70 eV): *m/z* (%): 358 (100) $[TTF(py)_2]$, 382 (31) [[FeL1]], 179 (69) $[C_8H_5NS_2]$, 103 (97) $[C_3H_3S_2]$, 76 (21) $[C_6H_4]$.

Synthesis in Acetonitrile (1b): A suspension of $[FeL1(MeOH)_2]$ (0.21 g, 0.47 mmol) and $TTF(py)_2$ (0.18 g, 0.50 mmol) in acetonitrile (20 mL) was heated to reflux for 3 h. After cooling and leaving to stand at room temperature for 2 d, the red powder was filtered off. The precipitate was washed with acetonitrile three times (3 mL) and dried in vacuo to give $\{[FeL1(TTF(py)_2)]\}_n$ (yield 0.19 g, 52.58 %) $C_{35}H_{30}FeN_4O_4S_4$ (754.05 g·mol^{-1}): calcd. C 55.70, H 4.01, N 7.42, S 16.99; found: C 55.18, H 3.76, N 7.48, S 16.96 %. **MS** (DEI-(+), 70 eV): *m/z* (%): 358 (100) $[TTF(py)_2]$, 382 (56) [[FeL1]], 179 (57) $[C_8H_5NS_2]$, 103 (97) $[C_3H_3S_2]$.

Synthesis in Ethanol (1c): A solution of [FeL1(MeOH)$_2$] (0.14 g, 0.31 mmol) and TTF(py)$_2$ (0.12 g, 0.33 mmol) in ethanol (30 mL) was heated to reflux for 4 h. After cooling and leaving to stand at 8 °C for 24 h, a dark red solid precipitated. The dark reddish powder was filtered off, washed with methanol two times (2 mL) and dried in vacuo to give {[FeL1(TTF(py)$_2$)]}$_n$ (yield 0.09 g, 41.3 %) $C_{35}H_{30}FeN_4O_4S_4$ (754.05 g·mol^{-1}): calcd. C 55.70, H 4.01, N 7.42, S 16.99 %; found: C 54.70, H 3.98, N 7.69, S 17.41 %. **MS** (DEI-(+), 70 eV): *m/z* (%): 358 (100) [TTF(py)$_2$], 382 (25) [[FeL1]], 179 (58) [$C_8H_5NS_2$], 103 (97) [$C_3H_3S_2$].

{[FeL2(TTF(py)$_2$)]}$_n$

Synthesis in DMF (2a): A solution of [FeL2(MeOH)$_2$] (0.28 g, 0.58 mmol) and TTF(py)$_2$ (0.22 g, 0.62 mmol) in DMF (20 mL) was heated to reflux for 2.5 h. After cooling and leaving to stand at room temperature for 3 d, a dark reddish powder was filtered off, washed with methanol three times (2 mL) and dried in vacuo to give {[FeL1(TTF(py)$_2$)]}$_n$ (yield 0.25 g, 58.2 %) $C_{34}H_{28}FeN_4O_6S_4$ (772.02 g·mol^{-1}): calcd. C 52.85, H 3.65, N 7.25, S 16.60 %; found: C 52.16, H 3.88, N 7.88, S 16.19 %. **MS** (DEI-(+), 70 eV): *m/z* (%): 415 (98) [FeL2], 359 (100) [TTF(py)$_2$], 179 (33) [$C_8H_5NS_2$], 103 (75) [$C_3H_3S_2$].

Preparation of C2a: A solution of [FeL2(MeOH)$_2$] (0.20 g, 0.42 mmol) and TTF(py)$_2$ (0.16 g, 0.44 mmol) in DMF (20 mL) was heated to reflux for 3 h. After cooling and leaving to stand at room temperature for 3 d some fine black crystals precipitated. An attempt to filter them failed due to insufficient amounts of solid particles present. The reagent solution was mixed with 2 mL methanol and stored at –38 °C. After 6 days crystals were obtained, which are suitable for single crystal structure analysis.

Synthesis in Acetonitrile (2b): A suspension of [FeL2(MeOH)$_2$] (0.20 g, 0.41 mmol) and TTF(py)$_2$ (0.16 g, 0.44 mmol) in acetonitrile (25 mL) was heated to reflux for 3 h and 15 min. After cooling and leaving to stand at room temperature for 2 d, a red powder was filtered off. The precipitate was washed with acetonitrile three times (3 mL) and dried in vacuo to give {[FeL2(TTF(py)$_2$)]}$_n$ (yield 0.21 g, 66.28 %) $C_{34}H_{28}FeN_4O_6S_4$ (772.02 g·mol^{-1}): calcd. C 52.85, H 3.65, N 7.25, S 16.60 %; found: C 52.2, H 3.71, N 7.06, S 16.55 %. **MS** (DEI-(+), 70 eV): *m/z* (%): 358 (100) [TTF(py)$_2$], 414 (31) [[FeL2]], 179 (67) [$C_8H_5NS_2$], 103 (97) [$C_3H_3S_2$], 76 (23) [C_6H_4]

Synthesis in Ethanol (2c): A solution of [FeL2(MeOH)$_2$] (0.2 g, 0.41 mmol) and TTF(py)$_2$ (0.16 g, 0.44 mmol) in ethanol (30 mL) was heated to reflux for 4 h. Upon heating, a dark red powder precipitated. After cooling and leaving to stand at room temperature for 1 d, a dark reddish powder was filtered off, washed with methanol three times (2 mL) and dried in vacuo to give {[FeL2(TTF(py)$_2$)]}$_n$ (yield 0.23 g, 72.7 %). $C_{34}H_{28}FeN_4O_6S_4$ (772.02 g·mol^{-1}): calcd. C 52.85, H 3.65, N 7.25, S 16.60 %; found: C 52.57, H 3.95, N 7.17, S 16.03 %. **MS** (DEI-(+), 70 eV): *m/z* (%): 358 (100) [TTF(py)$_2$], 414 (31) [[FeL2]], 179 (67) [$C_8H_5NS_2$], 103 (97) [$C_3H_3S_2$], 76 (23) [C_6H_4]

Supporting Information (see footnote on the first page of this article): Thermogravimetric Analysis of 1–c and 2a–c, Crystallographic data of C2a at 100 K and 273 K, Mössbauer spectra of 1a–c and 2a–b, PXRD pattern of 1a–c, Diffuse reflection spectrum of 2b and 2c, Diffuse reflection spectrum of pure 2a–c in NIR range, DFT-optimized structure of binuclear model **[(py)L1Fe(TTF(py)$_2$)FeL1(py)]** in the low spin/high spin state, S = 2, Character and energetic order of the highest occupied Mos, Cyclic voltammogram of 1a–c and 2a–c.

Acknowledgements

Financial support from the German Science Foundation (SFB840, A10) and the University of Bayreuth is gratefully acknowledged. Sophie Schönfeld thanks *Constantin Schreck* for preparing the single crystal of **2a** during a practical laboratory course. Open access funding enabled and organized by Projekt DEAL.

Keywords: Tetrathiafulvalene; Iron(II) complex; Iron; Spin crossover; Redox active

References

[1] a) E. Coronado, *Nat. Rev. Mater.* **2020**, *5*, 87–104; b) J. Ferrando-Soria, J. Vallejo, M. Castellano, J. Martínez-Lillo, E. Pardo, J. Cano, I. Castro, F. Lloret, R. Ruiz-García, M. Julve, *Coord. Chem. Rev.* **2017**, *339*, 17–103; c) B. Sieklucka, D. Pinkowicz (Eds.) *Molecular Magnetic Materials*, Wiley-VCH Verlag GmbH & Co. KGaA, Weinheim, Germany **2017**.

[2] A. Enriquez-Cabrera, A. Rapakousiou, M. Piedrahita Bello, G. Molnár, L. Salmon, A. Bousseksou, *Coord. Chem. Rev.* **2020**, *419*, 213396.

[3] B. Weber, *Coord. Chem. Rev.* **2009**, *253*, 2432–2449.

[4] a) A. Bousseksou, G. Molnár, L. Salmon, W. Nicolazzi, *Chem. Soc. Rev.* **2011**, *40*, 3313–3335; b) M. A. Halcrow (Ed.) *Spin-crossover materials. Properties and Applications*, Wiley, Chichester **2013**; c) S. Brooker, *Chem. Soc. Rev.* **2015**, *44*, 2880–2892; d) K. Senthil Kumar, Y. Bayeh, T. Gebretsadik, F. Elemo, M. Gebrezgiabher, M. Thomas, M. Ruben, *Dalton Trans.* **2019**, *48*, 15321–15337.

[5] K. Senthil Kumar, M. Ruben, *Coord. Chem. Rev.* **2017**, *346*, 176–205.

[6] V. Martínez, A. B. Gaspar, M. C. Muñoz, R. Ballesteros, N. Ortega-Villar, V. M. Ugalde-Saldívar, R. Moreno-Esparza, J. A. Real, *Eur. J. Inorg. Chem.* **2009**, *2009*, 303–310.

[7] S. Zein, S. A. Borshch, *J. Am. Chem. Soc.* **2005**, *127*, 16197–16201.

[8] a) H. Kurz, C. Lochenie, K. G. Wagner, S. Schneider, M. Karg, B. Weber, *Chem. Eur. J.* **2018**, *24*, 5100–5111; b) C. Lochenie, K. Schötz, F. Panzer, H. Kurz, B. Maier, F. Puchtler, S. Agarwal, A. Köhler, B. Weber, *J. Am. Chem. Soc.* **2018**, *140*, 700–709; c) J.-Y. Ge, Z. Chen, L. Zhang, X. Liang, J. Su, M. Kurmoo, J.-L. Zuo, *Angew. Chem. Int. Ed.* **2019**, *58*, 8789–8793; d) B. Benaicha, K. van Do, A. Yangui, N. Pittala, A. Lusson, M. Sy, G. Bouchez, H. Fourati, C. J. Gómez-García, S. Triki et al., *Chem. Sci.* **2019**, *10*, 6791–6798; e) M. Estrader, J. Salinas Uber, L. A. Barrios, J. Garcia, P. Lloyd-Williams, O. Roubeau, S. J. Teat, G. Aromí, *Angew. Chem. Int. Ed.* **2017**, *56*, 15622–15627.

[9] a) J. Weihermüller, S. Schlamp, W. Milius, F. Puchtler, J. Breu, P. Ramming, S. Hüttner, S. Agarwal, C. Göbel, M. Hund et al., *J. Mater. Chem. C* **2019**, *7*, 1151–1163; b) A. B. Gaspar, M. Seredyuk, *Coord. Chem. Rev.* **2014**, *268*, 41–58; c) T. Romero-Morcillo, M. Seredyuk, M. C. Muñoz, J. A. Real, *Angew. Chem. Int. Ed.* **2015**, *54*, 14777–14781; d) C. Gandolfi, T. Cotting, P. N. Martinho, O. Sereda, A. Neels, G. G. Morgan, M. Albrecht, *Dalton Trans.* **2011**, *40*, 1855–1865; e) Y. Komatsu, K. Kato, Y. Yamamoto, H. Kamihata, Y. H. Lee, A. Fuyuhiro, S. Kawata, S. Hayami, *Eur. J. Inorg. Chem.* **2012**, *2012*, 2769–2775.

[10] H.-Y. Wang, L. Cui, J.-Z. Xie, C. F. Leong, D. M. D'Alessandro, J.-L. Zuo, *Coord. Chem. Rev.* **2017**, *345*, 342–361.

[11] a) M. Schwarz, A. Zamir, U. Pick, *J. Plant Nutrition* **2003**, *26*, 2081–2091; b) L. Hu, W. Liu, C.-H. Li, X.-H. Zhou, J.-L. Zuo, *Eur. J. Inorg. Chem.* **2013**, *2013*, 6037–6048; c) F. Shen, W. Huang, D. Wu, Z. Zheng, X.-C. Huang, O. Sato, *Inorg. Chem.* **2016**, *55*, 902–908.

[12] J.-F. Létard, P. Guionneau, L. Goux-Capes, in: *Topics in Current Chemistry*, *Vols. 235* (Eds.: P. Gütlich, H. A. Goodwin), Springer, Berlin, Heidelberg **2004**, 221–249.
[13] S. Schönfeld, K. Dankhoff, D. Baabe, M.-K. Zaretzke, M. Bröring, K. Schötz, A. Köhler, G. Hörner, B. Weber, *Inorg. Chem.* **2020**, *59*, 8320–8333.
[14] Y.-R. Qiu, L. Cui, P.-Y. Cai, F. Yu, M. Kurmoo, C. F. Leong, D. M. D′Alessandro, J.-L. Zuo, *Chem. Sci.* **2020**, *11*, 6229–6235.
[15] D. Canevet, M. Sallé, G. Zhang, D. Zhang, D. Zhu, *Chem. Commun.* **2009**, 2245–2269.
[16] J. Ferraris, D. O. Cowan, V. Walatka, J. H. Perlstein, *J. Am. Chem. Soc.* **1973**, *95*, 948–949.
[17] J. O. Jeppesen, M. B. Nielsen, J. Becher, *Chem. Rev.* **2004**, *104*, 5115–5132.
[18] B. Weber, E.-G. Jäger, *Eur. J. Inorg. Chem.* **2009**, *2009*, 465–477.
[19] a) B. Weber, F. A. Walker, *Inorg. Chem.* **2007**, *46*, 6794–6803; b) W. Bauer, M. M. Dîrtu, Y. Garcia, B. Weber, *CrystEngComm* **2012**, *14*, 1223–1231.
[20] R. Nowak, W. Bauer, T. Ossiander, B. Weber, *Eur. J. Inorg. Chem.* **2013**, *2013*, 975–983.
[21] S. Schönfeld, C. Lochenie, G. Hörner, B. Weber, *J. Phys.: Condens. Matter* **2019**, *31*, 504002.
[22] Y.-F. Han, J.-S. Zhang, Y.-J. Lin, J. Dai, G.-X. Jin, *J. Organomet. Chem.* **2007**, *692*, 4545–4550.
[23] R. Wang, L.-C. Kang, J. Xiong, X.-W. Dou, X.-Y. Chen, J.-L. Zuo, X.-Z. You, *Dalton Trans.* **2011**, *40*, 919–926.
[24] L. Zappe, S. Schönfeld, G. Hörner, K. A. Zenere, C. F. Leong, C. J. Kepert, D. M. D'Alessandro, B. Weber, S. M. Neville, *Chem. Commun.* **2020**, *56*, 10469–10472.
[25] Q.-Y. Zhu, L.-B. Huo, Y.-R. Qin, Y.-P. Zhang, Z.-J. Lu, J.-P. Wang, J. Dai, *J. Phys. Chem. B* **2010**, *114*, 361–367.
[26] a) O. Paz-Tal Levi, J. Y. Becker, A. Ellern, V. Khodorkovsky, *Tetrahedron Lett.* **2001**, *42*, 1571–1573; b) E. Cerrada, J. Garrido, M. Laguna, N. Lardiés, I. Romeo, *Synth. Met.* **1999**, *102*, 1709–1710.
[27] a) W. Bauer, T. Ossiander, B. Weber, *Z. Naturforsch. B* **2010**, *65*, 323–328; b) E.-G. Jger, E. Hussler, M. Rudolph, A. Schneider, *Z. Anorg. Allg. Chem.* **1985**, *525*, 67–85.
[28] V. Gutmann, *Angew. Chem. Int. Ed. Engl.* **1970**, *9*, 843–860.
[29] F. Arnaud-Neu, R. Delgado, S. Chaves, *Pure Appl. Chem.* **2003**, *75*, 71–102.
[30] a) Q. Yu, J. Su, J.-P. Ma, C. F. Leong, D. M. D'Alessandro, H.-Y. Wang, M. Kurmoo, J.-L. Zuo, *Cryst. Growth Des.* **2019**, *19*, 3012–3018; b) L. Wang, B. Zhang, J. Zhang, *Inorg. Chem.* **2006**, *45*, 6860–6863.
[31] a) F. Iwahori, S. Golhen, L. Ouahab, R. Carlier, J. P. Sutter, *Inorg. Chem.* **2001**, *40*, 6541–6542; b) C. Jia, S.-X. Liu, C. Ambrus, A. Neels, G. Labat, S. Decurtins, *Inorg. Chem.* **2006**, *45*, 3152–3154.
[32] H. Kobayashi, R. Kato, T. Mori, A. Kobayashi, Y. Sasaki, G. Saito, T. Enoki, H. Inokuchi, *Mol. Crystals Liquid Crystals* **1984**, *107*, 33–43.
[33] a) G. Kortüm, W. Braun, G. Herzog, *Angew. Chem. Int. Ed. Engl.* **1963**, *2*, 333–341; b) G. Kortüm, G. Schreyer, *Angew. Chem.* **1955**, *67*, 694–698.
[34] M. Parthey, M. Kaupp, *Chem. Soc. Rev.* **2014**, *43*, 5067–5088.
[35] E.-G. Jäger, E. Häussler, M. Rudolph, A. Schneider, *Z. Anorg. Allg. Chem.* **1985**, *525*, 67–85.
[36] D. A. C. Brownson, C. E. Banks (Eds.) *The Handbook of Graphene Electrochemistry*, Springer London, London **2014**.
[37] Y. Hou, Y. Chen, Q. Liu, M. Yang, X. Wan, S. Yin, A. Yu, *Macromolecules* **2008**, *41*, 3114–3119.
[38] a) O. Klimm, C. Göbel, S. Rosenfeldt, F. Puchtler, N. Miyajima, K. Marquardt, M. Drechsler, J. Breu, S. Förster, B. Weber, *Nanoscale* **2016**, *8*, 19058–19065; b) C. Göbel, C. Hils, M. Drechsler, D. Baabe, A. Greiner, H. Schmalz, B. Weber, *Angew. Chem. Int. Ed.* **2020**, *59*, 5765–5770.
[39] a) G. M. Sheldrick, *Acta Crystallogr., Sect. A Struct. Chem.* **2008**, *64*, 112–122; b) G. M. Sheldrick, *Acta Crystallogr., Sect. C Struct. Chem.* **2015**, *71*, 3–8.
[40] O. V. Dolomanov, L. J. Bourhis, R. J. Gildea, J. A. K. Howard, H. Puschmann, *J. Appl. Crystallogr.* **2009**, *42*, 339–341.

Received: July 31, 2020
Published Online: ■

Journal of Inorganic and General Chemistry
ZAAC
Zeitschrift für anorganische und allgemeine Chemie

ARTICLE